

Percolation analysis of the atmospheric structure

Yu Sun,¹ Jun Meng,^{2,3,*} Qing Yao,¹ Abbas Ali Saberi,^{4,5} Xiaosong Chen ,¹ Jingfang Fan ,^{1,3,†} and Jürgen Kurths^{3,6}

¹*School of Systems Science, Beijing Normal University, 100875 Beijing, China*

²*School of Science, Beijing University of Posts and Telecommunications, Beijing 100876, China*

³*Potsdam Institute for Climate Impact Research, 14412 Potsdam, Germany*

⁴*Department of Physics, University of Tehran, Tehran 14395-547, Iran*

⁵*Institut für Theoretische Physik, Universität zu Köln, Zùlpicher Strasse 77, 50937 Köln, Germany*

⁶*Department of Physics, Humboldt University, 10099 Berlin, Germany*



(Received 10 March 2021; accepted 10 December 2021; published 28 December 2021)

The atmosphere is a thermo-hydrodynamical complex system and provides oxygen to most animal life at the Earth's surface. However, the detection of complexity for the atmosphere remains elusive and debated. Here we develop a percolation-based framework to explore its structure by using the global air temperature field. We find that the percolation threshold is much delayed compared with the prototypical percolation model and the giant cluster eventually emerges explosively. A finite-size-scaling analysis reveals that the observed transition in each atmosphere layer is genuine discontinuous. Furthermore, at the percolation threshold, we uncover that the boundary of the giant cluster is self-affine, with fractal dimension d_f , and can be utilized to quantify the atmospheric complexity. Specifically, our results indicate that the complexity of the atmosphere decreases superlinearly with height, i.e., the complexity is higher at the surface than at the top layer and vice versa, due to the atmospheric boundary forcings. The proposed methodology may evaluate and improve our understanding regarding the critical phenomena of the complex Earth system and can be used as a benchmark tool to test the performance of Earth system models.

DOI: [10.1103/PhysRevE.104.064139](https://doi.org/10.1103/PhysRevE.104.064139)

I. INTRODUCTION

The Earth behaves as a complex and adaptive system that contains two main components: the ecosphere as well as the human factor [1]. The development of Earth system science has achieved a deep integration of biosphere, geosphere, and human dynamics to build a unified understanding of the Earth system [2]. During its evolution, some new concepts such as sustainability [3], anthropocene [4], and planetary boundaries framework [5] have arisen. In particular, the terms of tipping elements [6] were introduced to describe the Earth, which is a large-scale system that may pass a *tipping point*. Recently, Lenton *et al.* highlighted that nine climate tipping points, such as the collapse of the Greenland ice sheet, the loss of the Amazon rainforest and the slowdown of the Atlantic Meridional Overturning Circulation have been activated in the past decade [7], and therefore urgent action to reduce greenhouse gas emissions to prevent key tipping points should be taken. Critical phenomena in physics are analogous to the tipping elements in Earth science [8], where a system will collapse and follow a breakdown, if it is close to a phase-transition point [9,10]. They are among the most striking phenomena of nature and society [11]. The atmosphere, as one of the main components of Earth, plays a vital role in the function and sustainability of the Earth's system. Peters and Neelin pointed out

that the atmospheric convection and precipitation behave as a critical phenomenon with water vapor as the tuning parameter [12].

Percolation, a basic example of a critical phenomenon, describes a geometrical phase transition where the critical concentration separates a phase of finite clusters from a phase where an infinite (or giant) cluster is present [13,14]. It further becomes an effective tool for studying the structure, robustness, and function of complex systems [15,16] and has been a cornerstone in the theory of spatial stochastic processes with broad applications such as epidemiology [17–19], networks [20–23], turbulence [24], and traffic [25]. It has also been successfully implemented in Earth sciences, for instance, to study the critical behavior of transport in sea ice [26], to analyze the global patterns of tropical forest fragmentation [27], to investigate the geometrical features of Earth [28,29], to predict the occurrence of extreme climate events [30] and impacts of climate change [31], etc. [32]. In this Letter, we apply percolation theory to unveil the criticality, complexity, and structure of the atmosphere. Generally speaking, the atmosphere exhibits irregular variations and fluctuations, and is composed of four concentric layers: the troposphere, stratosphere, mesosphere, and thermosphere [33]. About 99% of the total atmospheric mass is concentrated in the first 30 km above Earth's surface. The complexity of the atmosphere is mainly driven by physical processes, such as radiation, convection, and aerosol movement. Figure 1 depicts the atmospheric wind circulation patterns within different pressure levels, i.e., from top to surface, 10, 850, and 1000 hPa, respectively.

*Corresponding author: junmeng@bupt.edu.cn

†jingfang@bnu.edu.cn

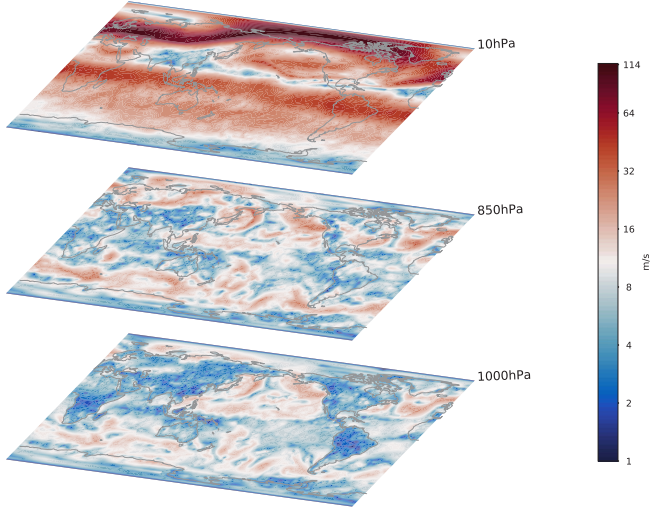


FIG. 1. Schematic of atmospheric wind circulation patterns for different pressure levels, from top to bottom, 10, 850, and 1000 hPa, respectively. Here we chose the wind speed (m/s) data from January 1, 2020.

We find that the structure and circulation patterns are quite complex and different from each other. It was reported that the complex nonlinear atmospheric dynamics cascaded from planetary scales down to small viscous scales [34]. There are many nonequilibrium dynamic phenomena that must be analyzed to completely understand the atmosphere [35].

II. DATA AND METHODS

Our analysis is based on global monthly mean-air-temperature data with as many as 37 vertical pressure levels from the European Centre for Medium-range Weather Forecasts (ECMWF) ERA5 reanalysis datasets [36]. The searching principle for air-temperature data is as follows: (i) It is the most commonly measured weather or climate parameter and describes the kinetic energy, or energy of motion, of the gases that make up air. (ii) Temperature varies greatly at different heights relative to the Earth's surface and characterizes different layers of the atmosphere. More specifically, each layer represents a special meteorological meaning, e.g., 1000 hPa stands for the near surface level; 850 hPa temperature is approximately 1.5 km above sea level, usually just above the boundary layer, and is used to locate and identify warm and cold fronts; 200 hPa is the upper boundary of the troposphere (top of the troposphere), the temperature generally decreases with increasing height up to the troposphere; 1 hPa means the top layer of the stratosphere, which is approximately 50 km above sea level. For each layer of the atmosphere, the temperature field is divided into N grids (nodes) with resolution $r = 0.25^\circ$, resulting in $N = 721 \times 1440$, where 721 is the number of grids in the meridional (north-south) direction, and 1440 is the number of grids in the zonal (east-west) direction. Due to the Earth's spherical shape, the grids at different latitudes represent different area, i.e., proportional to $\cos(\phi)$, where ϕ is the latitude. We therefore define the reduced area for each

site i at latitude ϕ_i as

$$s_i = \frac{\cos(\phi_i)}{\sum_{j=1}^N \cos(\phi_j)}. \quad (1)$$

The time period spans from 1979 to 2020 (the data can be downloaded from Ref. [37]).

Data filtering. To avoid the strong effect of seasonality, we subtract the mean seasonal cycle over 42 years. For each node or grid i (i.e., longitude-latitude grid point), we calculate the monthly atmospheric temperature anomalies $\tilde{T}_i(t) = T_i(t) - \langle T_i \rangle$, where $T_i(t)$ is the actual temperature value, $\langle T_i \rangle$ stands for the climatological average at the given node i , and t is the time. We then define the standard deviation $\mathcal{R}_i = \text{std}(\tilde{T}_i(t))$ as the climate variance at node i , which quantifies the deviation or variation of real temperature from the mean seasonal cycle. The spatial structure of the air-temperature anomalies standard deviation field \mathcal{R}_i varies between different pressure levels [see, e.g., Figs. 2(a)–2(c)], reflecting different atmosphere-ocean-land interaction processes, is thus a good indicator of atmosphere complexity. It reveals some climate modes and patterns, e.g., the ENSO and the Antarctic circumpolar current, as shown in Fig. 2(a).

Percolation model. We first rank all the nodes according to their climate variance \mathcal{R}_i , from the largest to the smallest value (see Fig. 2). Our percolation model is defined as follows: starting from an unoccupied node (or site) on a lattice network embedded in two dimensions (2D), the nodes are occupied one by one according to their ranking, i.e., we first choose and add the node with the highest \mathcal{R}_i , then the second, etc. Second, we identify the clusters based on classical percolation theory: a cluster is a subset of nearest-neighbor nodes such that there exists at least one path from each node in the subset to another [16,38]. Here we use the efficient Newman–Ziff algorithm to detect the different clusters in evolving progress [39]. In this study, sites are indeed defined as latitude-longitude grids, with resolution $r = 0.25^\circ$ on this sphere. Since our Earth is spherical in shape, i.e., the sites at latitude 90° S (south pole) and latitude 90° N (north pole) are not adjacent, therefore, free boundary conditions are adopted along the north-south direction. However, the sites at longitude 0° and longitude 360° are actually the same, thus, periodic boundary conditions are adopted along the east-west direction. Therefore, each node has four nearest neighbors (except the north and south poles). Besides, we perform a percolation analysis of the atmospheric structure, and we do not consider Earth's surface, i.e., covered by water (i.e., oceans) or land. In percolation theory, the relative size of the largest cluster is usually defined as the order parameter [13]. Different from classical percolation theory due to the Earth's spherical shape, the largest cluster s in the atmospheric system is redefined as [31] according to Eq. (1):

$$s = \max \left[\left(\sum_{i \in \mathcal{H}_1} s_i \right), \left(\sum_{i \in \mathcal{H}_2} s_i \right), \dots, \left(\sum_{i \in \mathcal{H}_m} s_i \right), \dots \right], \quad (2)$$

where \mathcal{H}_m denotes a series of disjoint subnetworks. During the evolution of our atmospheric system, we measure the order parameter $s(P)$ at time step P and compute its relative largest

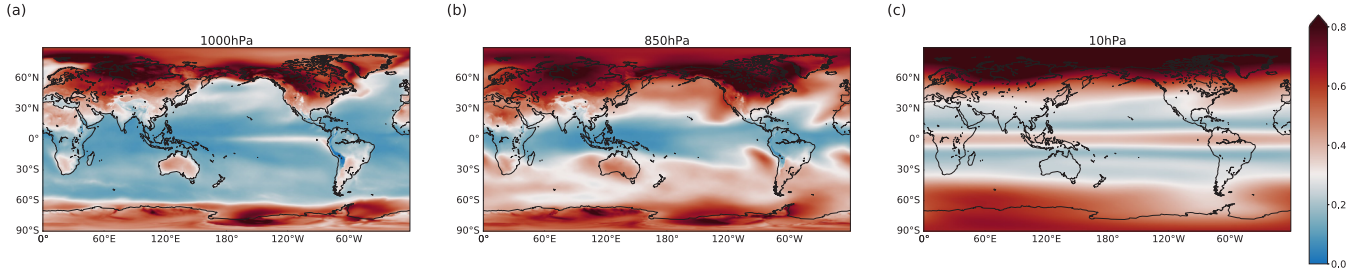


FIG. 2. Illustration of air temperature anomaly spatial standard deviation \mathcal{R}_i maps for three specific pressure levels: (a) 1000 hPa, (b) 850 hPa, and (c) 10 hPa. \mathcal{R} quantifies the deviation or variation of real temperature from the mean seasonal cycle for each pressure level. Here \mathcal{R} is normalized from 0 to 1.

one-step gap Δ [40,41]:

$$\Delta \equiv \max_p (s[P+1] - s[P]). \quad (3)$$

Meanwhile, we define the occupied probability $p = P/N$, the time step with the largest jump Δ as P_c and the corresponding reduced transition point as $p_c = P_c/N$. Equation (3) is used to determine the percolation threshold. As explained in the following, our results indicate that the percolation model undergoes an abrupt and explosive phase transition at the critical threshold p_c , with a significant discontinuity in the order parameter s (shown in Fig. 3).

III. RESULTS

Figure 3(a) shows the atmospheric (1000 hPa) network cluster structure in the color map at the percolation threshold p_c [indicated by the dashed line in Fig. 3(b)]. We find that the network is characterized by two major compact communities: the largest one is located in the Northern Hemisphere (red color) and the second-largest one in the Southern Hemisphere (blue color). In the next step, a critical node will add and merge the two clusters, resulting in the formation of a supergiant component. Figure 3(b) depicts the relative size of the largest cluster s as a function of p . It shows that s undergoes an abrupt jump at the percolation threshold $p_c \approx 0.76$, which is much delayed compared with the prototypical site percolation model, $p_c \approx 0.593$ [39]. This p_c describes the tipping point at which the atmospheric system switches from several smaller clusters to very fewer larger ones. Each cluster had similar climate phenomenon. This finding allows us to relate changes in the cluster structure of the climate system to more specific phenomena. For example, the clusters can capture the El Niño Southern Oscillation (ENSO) pattern very well; see the central and eastern equatorial Pacific in Fig. 3(a). ENSO is one of the most influential coupled ocean-atmosphere climate phenomena, occurring about every two to seven years [42]. To verify our conjecture, we perform the same analysis for every five years separately. The results are shown in Fig. S1 of the Supplemental Materials [43] and we find that the ENSO pattern only appears in the period including very strong El Niño events (1982–1983, 1997–1998, and 2014–2016) as well as strong La Niña events (2007–2008 and 2010–2011).

Figures 3(c) and 3(d) illustrate the atmospheric cluster structure at the percolation threshold, and the evolution of s at the 850 hPa pressure level. Likewise, we also observe an abrupt percolation phase transition. However, there are some

substantial differences for the atmospheric cluster structure between 1000 and 850 hPa: The ENSO pattern disappears [Fig. 3(c)] because of the weakening ocean-atmosphere interactions from the surface layer [44,45]. For the case of 10 hPa, we demonstrate the results in Figs. 3(e) and 3(f). To better understand the temperature mode and the dynamic percolation progress in different pressure levels, we show six nodes worth of temperature in Fig. S2 and illustrate the dynamical evolution of percolation in the Movies S1–S3 (see Supplemental Materials [43]).

The order of the phase transition is a fundamental property in critical phenomenon. A lattice or network system is expected to undergo a continuous percolation phase transition during a random occupation or failure process [46]. To demonstrate that the observation of the jump Δ in the order parameter is genuinely discontinuous, we study the finite-size effects of our atmospheric system by altering the resolution of nodes, i.e., we increase the resolution from $r = 0.25^\circ$ to 0.5° , resulting in $L = 1440$ to 720 , etc. Note that, in this progress, we do not change or rescale the real data (not reproduce new data). We then calculate $\Delta(L)$, see Eq. (3), the largest gap in s as a function of network system size L and see how it behaves when extrapolated to infinite system size. Following Ref. [41], $\Delta(L)$ is anticipated to exhibit a scaling relation, as a function of system size L ,

$$\Delta(L) \sim L^{-\beta_1}, \quad (4)$$

where β_1 is the critical exponent characterizing the universality class of the percolation problem. The value of β_1 indicates the order of the percolation, i.e., $\beta_1 = 0$ immediately implies a discontinuous percolation transition; otherwise, $\beta_1 > 0$ implies the continuity of the phase transition. Figure 4(a) presents the order parameter s as a function of the occupied probability p with different system sizes $L = 1440, 720, 360$, and 180 . Our results suggest that there are no significant finite-size effects for our model, since the three curves are nearly overlapping. In addition, Fig. 4(b) reveals that $\beta_1 = 0$, indicating Δ tends to be a nonzero constant as $L \rightarrow \infty$.

Null model. To demonstrate that the discontinuity in our atmospheric percolation model is not accidental, we propose a *null model*. The null model is numerically generated by shuffling the surrogate of the original data. We have realized 10 000 such randomizations and performed the percolation in each sample. This procedure destroys the spatial association in the standard deviation (\mathcal{R}_i) profile, while it keeps its distribution (see Fig. S3 of the Supplemental Material

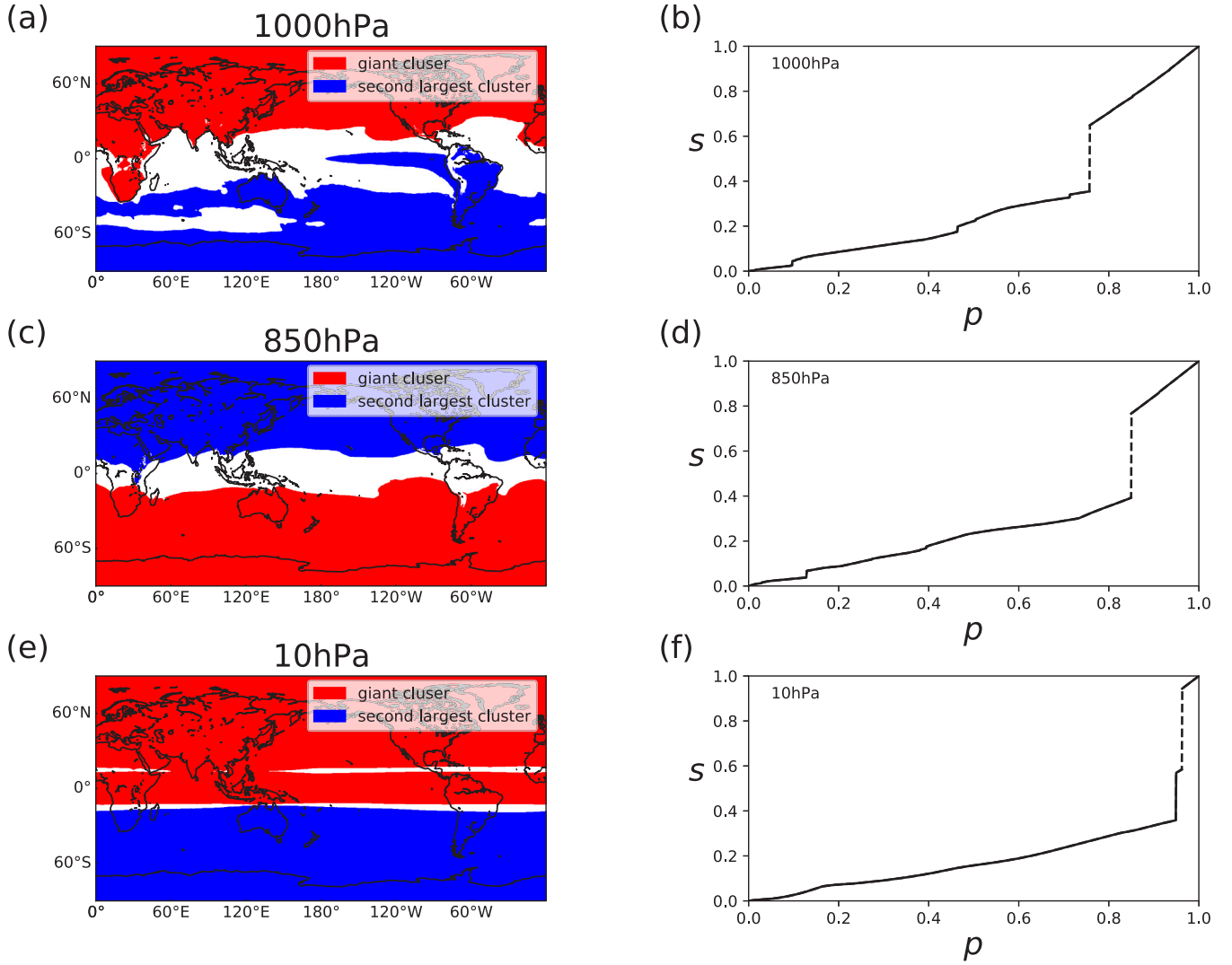


FIG. 3. Snapshots of the atmospheric percolation cluster structures. (a) Plot of the giant (red) and second-largest (blue) clusters just before the percolation threshold $p_c \approx 0.76$ for 1000 hPa pressure layer. (b) Schematic plot of the largest cluster size s versus the occupied probability p , the number of attached nodes per N for the percolation model. Analogous to panels (a) and (b), panels (c) and (d) show the case of the 850 hPa pressure layer, and panels (e) and (f) show the case of the 10 hPa pressure layer. The grid resolution is 0.25° , resulting in $L = 1440$, and $N = 1440 \times 721$. The dashed lines in panels (b), (d), and (f) indicate the corresponding percolation threshold.

[43]). As expected, the shuffled samples all correspond to the classical uncorrelated site percolation class [39] with a continuous phase transition at $p \approx 0.59$, and critical exponent $\beta_1 = 15/144 \approx 0.104$ [41], as shown in Fig. 4. For the case of other pressure levels, 850 and 10 hPa, we observe similar results that are shown in Fig. S4 of the Supplemental Material [43].

In the following, we analyze the fractal dimension of the percolation cluster and use it to quantify the complexity of the atmosphere. The fractal concept was first introduced by Mandelbrot [47] and applied to percolation by Stanley [48]. It is used to describe the cluster shapes at the percolation threshold p_c . The giant cluster is self-similar on all length scales and can be regarded as a fractal. Here, we consider the boundary (interface) of the largest cluster at the percolation threshold (as shown in Fig. S5 of the Supplemental Material [43]) and define N_b as the number of nodes in this boundary. The fractal dimension d_f can be estimated by examining the

following power-law fit:

$$N_b(L) \sim L^{d_f}. \quad (5)$$

The value of d_f indicates the self-similar fractal patterns and complexity of a system, such as coast lines [49]. The goodness of fit, as shown in Fig. 5(a), provides excellent support for Eq. (5), suggesting that the boundary of the largest cluster is self-affine. Figure 5(b) shows the value of d_f for all 37 pressure levels. We uncover that d_f generally increases superlinearly with pressure \mathcal{P} because $d_f(\mathcal{P}) - 1 \sim \mathcal{P}^4$. This means that the complexity of the atmosphere is much higher on the surface (1000 hPa) than at the top (1 hPa). We associate the possible climatological and physical origin of the complexity with the atmospheric boundary forcings, i.e., solar radiation and ocean-surface and land conditions. The atmospheric state (winds, temperatures, humidities, etc.) is significantly affected by the exchange of energy and fluxes at the interface of the ocean (or land) and atmosphere through

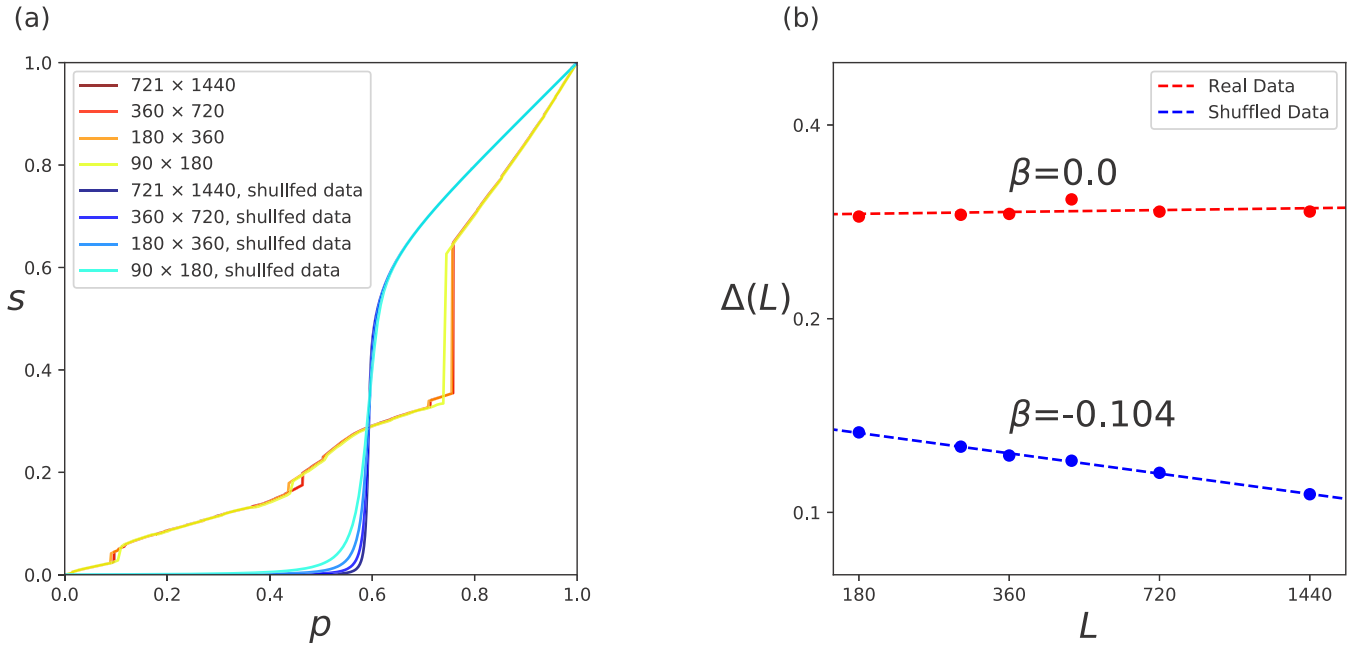


FIG. 4. Finite-size effects of the percolation for both real data and shuffled (null model) data. (a) The largest cluster size s plotted as a function of p with different system size. (b) Log-log plot of the size of the largest gap $\Delta(L)$ versus L . The dashed lines in panel (b) are best-fit lines for the data with $R^2 > 0.99$. Results for the null model are obtained over 10 000 independent realizations.

compensatory dynamical circulations [50]. Remarkably, these coupled interactions become weaker for higher layers and thus yielding a lower complexity.

The complex Earth system is modulated by both external (e.g., solar radiation, the sphericity of the earth, rotation, topography, vegetation cover, etc.) and internal factors (e.g., the intrinsic properties of the atmosphere, composition, various instabilities, and the general circulation). The numerical cli-

mate model is considered as the primary tool for investigating our Earth. It rests on the fundamental laws of physics, chemistry, and biology. However, there are still processes that it cannot emulate because (i) they are insufficiently understood or (ii) they occur on spatial-temporal scales which the model cannot capture. Our theoretical approach proposed here is based on the observed data and provides a fresh insight into the underlying mechanism of the Earth system. In particular,

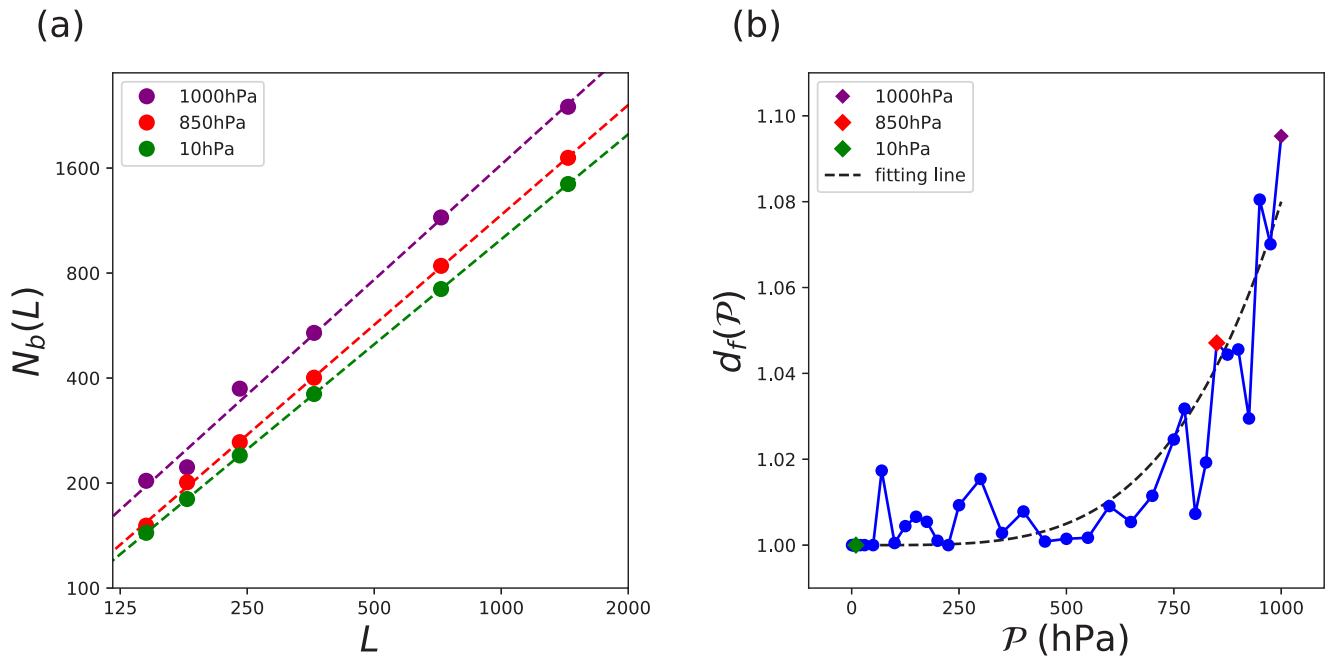


FIG. 5. (a) Log-log plot of the length of the boundary $N_b(L)$ versus L at the percolation threshold for 1000, 850, and 10 hPa pressure levels. The dashed lines are the best-fit lines for the data with $R^2 > 0.99$. (b) Plot of the fractal dimension $d_f(\mathcal{P})$ as a function of pressure level \mathcal{P} . The dashed line is a fitting line described by a quartic regression equation with $d_f(\mathcal{P}) = 1 + 8 \times 10^{-14} \mathcal{P}^4$.

it builds an essential parameter for quantifying complexity which can be used as a benchmark tool to test the performance of Earth system models.

To demonstrate that our method can be used as a benchmark tool to diagnose the climate system, we perform the same percolation analysis on the temperature field of the two Earth system models, i.e., the CMCC-CM model and the CNRM-CM5 model with the Representative Concentration Pathway 8.5 (RCP8.5) scenario in the Coupled Model Intercomparison Project Phase 5 (CMIP5) twenty-first century climate change simulations. The chosen principles for the models are as follows: (i) they must contain air temperature fields with different pressure layers, and (ii) they must have higher resolution. Resolutions are given as the number of latitude \times longitude grid points, e.g., CMCC-CM with 240×480 and CNRM-CM5 with 128×256 . The evolution of the largest cluster size S with increasing occupied probability is shown in Figs. S8 and S10 of the Supplemental Material [43] for the two models, respectively. The fractal dimension d_f as a function of pressure levels is also shown in Figs. S9 and S11. Compared with the over-served ERA5 reanalysis dataset, we find that both models undergo discontinuous percolation phase transitions for different layers. The fractal dimension for the CMCC-CM model exhibits an increasing trend with pressure levels, which indicates that the complexity of the atmosphere decreases with its height. However, for the CNRM-CM5 model, we do not find such a significant increasing trend [see Fig. S11(b)], in particular, for the lower pressure levels. Based on the diagnostic of complexity, we thus think further improvement is needed for the CNRM-CM5 model.

IV. DISCUSSIONS

In summary, the structure of the atmosphere governs the Earth's energy behavior and controls how the climate develops. It is thus of great importance that its better characteristics will improve our description and understanding of the Earth system. Here, we developed a percolation model that analyzes the atmospheric structure and its complexity in a systematic and quantitative way. Our method is based on the global air temperature with as many as 37 pressure levels. Specifically, we have observed an abrupt jump during the dynamical evolution of percolation; applying a finite-size scaling analysis, we have uncovered that the transition is genuine discontinuous. Furthermore, the fractal dimension of the largest cluster at the percolation threshold was introduced and used to measure the complexity of the atmosphere. The methodology proposed here provides two breakthroughs: (i) enriching the understanding of the discontinuous phase transition, in particular, the explosive percolation phenomenon as a practical model emerging in a natural dynamical system governing the global properties of Earth in connection with the time spread of global warming [51–56]. Some climate spatial patterns, such as ENSO and ocean currents, can produce a natural external bias to systematically suppress the formation of the largest cluster; (ii) assessing the quality and reliability of sophisticated climate models. Even though the models range from simple energy balance models to complex Earth system models, they can be very impressive and give good approximations to atmospheric behavior. However, they are not complete and true representations of the governing physics [57]. Our method allows us to enhance and improve the capacity building for addressing climate change.

-
- [1] H. J. Schellnhuber, ‘Earth system’ analysis and the second Copernican revolution, *Nature (London)* **402**, C19 (1999).
 - [2] W. Steffen *et al.*, The emergence and evolution of Earth System Science, *Nat. Rev. Earth Environ.* **1**, 54 (2020).
 - [3] W. C. Clark and R. E. Munn, *Sustainable Development of the Biosphere* (Cambridge University Press, Cambridge, 1986).
 - [4] P. J. Crutzen, Geology of mankind, *Nature (London)* **415**, 23 (2002).
 - [5] J. Rockström *et al.*, A safe operating space for humanity, *Nature (London)* **461**, 472 (2009).
 - [6] T. M. Lenton *et al.*, Tipping elements in the Earth’s climate system, *Proc. Natl. Acad. Sci. USA* **105**, 1786 (2008).
 - [7] T. M. Lenton *et al.*, Climate tipping points—too risky to bet against, *Nature (London)* **575**, 592 (2019).
 - [8] V. Lucarini and T. Bódi, Transitions across Melancholia States in a Climate Model: Reconciling the Deterministic and Stochastic Points of View, *Phys. Rev. Lett.* **122**, 158701 (2019).
 - [9] S. V. Buldyrev, R. Parshani, G. Paul, H. E. Stanley, and S. Havlin, Catastrophic cascade of failures in interdependent networks, *Nature (London)* **464**, 1025 (2010).
 - [10] J. Krönke *et al.*, Dynamics of tipping cascades on complex networks, *Phys. Rev. E* **101**, 042311 (2020).
 - [11] M. Scheffer, *Critical Transitions in Nature and Society* (Princeton University Press, Princeton, 2009).
 - [12] O. Peters and J. D. Neelin, Critical phenomena in atmospheric precipitation, *Nat. Phys.* **2**, 393 (2006).
 - [13] D. Stauffer and A. Aharony, *Introduction to Percolation Theory* (Taylor & Francis, London, 2003).
 - [14] A. A. Saberi, Recent advances in percolation theory and its applications, *Phys. Rep.* **578**, 1 (2015).
 - [15] K. Christensen and N. R. Moloney, *Complexity and Criticality* (World Scientific Publishing Company, London, 2005), Vol. 1.
 - [16] R. Cohen and S. Havlin, *Complex Networks: Structure, Robustness and Function* (Cambridge University Press, New York, 2010).
 - [17] M. E. J. Newman, S. H. Strogatz, and D. J. Watts, Random graphs with arbitrary degree distributions and their applications, *Phys. Rev. E* **64**, 026118 (2001).
 - [18] S. Davis, P. Trapman, H. Leirs, M. Begon, and J. A. P. Heesterbeek, The abundance threshold for plague as a critical percolation phenomenon, *Nature (London)* **454**, 634 (2008).
 - [19] P.-S. Romualdo, C. Castellano, P. Van Mieghem, and A. Vespignani, Epidemic processes in complex networks, *Rev. Mod. Phys.* **87**, 925 (2015).

- [20] D. S. Callaway, M. E. J. Newman, S. H. Strogatz, and D. J. Watts, Network Robustness and Fragility: Percolation on Random Graphs, *Phys. Rev. Lett.* **85**, 5468 (2000).
- [21] I. Derényi, G. Palla, and T. Vicsek, Clique Percolation in Random Networks, *Phys. Rev. Lett.* **94**, 160202 (2005).
- [22] J. Gao, S. V. Buldyrev, H. E. Stanley, and S. Havlin, Networks formed from interdependent networks, *Nat. Phys.* **8**, 40 (2012).
- [23] F. Radicchi and A. Arenas, Abrupt transition in the structural formation of interconnected networks, *Nat. Phys.* **9**, 717 (2013).
- [24] D. Bernard, G. Boffetta, A. Celani, and G. Falkovich, Conformal invariance in two-dimensional turbulence, *Nat. Phys.* **2**, 124 (2006).
- [25] D. Li *et al.*, Percolation transition in dynamical traffic network with evolving critical bottlenecks, *Proc. Natl. Acad. Sci. USA* **112**, 669 (2015).
- [26] K. M. Golden, S. F. Ackley, and V. I. Lytle, The Percolation Phase Transition in Sea Ice, *Science* **282**, 2238 (1998).
- [27] F. Taubert *et al.*, Global patterns of tropical forest fragmentation, *Nature (London)* **554**, 519 (2018).
- [28] A. Ali Saberi, Percolation Description of the Global Topography of Earth and the Moon, *Phys. Rev. Lett.* **110**, 178501 (2013).
- [29] J. Fan, J. Meng, and A. A. Saberi, Percolation framework of the Earth's topography, *Phys. Rev. E* **99**, 022304 (2019).
- [30] J. Meng, J. Fan, Y. Ashkenazy, and S. Havlin, Percolation framework to describe El Niño conditions, *Chaos* **27**, 035807 (2017).
- [31] J. Fan, J. Meng, Y. Ashkenazy, S. Havlin, and H. J. Schellnhuber, Climate network percolation reveals the expansion and weakening of the tropical component under global warming, *Proc. Natl. Acad. Sci. USA* **115**, E12128 (2018).
- [32] J. Fan *et al.*, Statistical physics approaches to the complex Earth system, *Phys. Rep.* **896**, 1 (2021).
- [33] D. S. Wilks, *Statistical Methods in the Atmospheric Sciences* (Academic Press, London, 2011), Vol. 100.
- [34] L. F. Richardson, Atmospheric diffusion shown on a distance-neighbour graph, *Proc. R. Soc. London Ser. A* **110**, 709 (1926).
- [35] J. P. Peixoto and A. H. Oort, *Physics of Climate*, 1st ed. (American Institute of Physics, New York, 1992).
- [36] D. P. Dee *et al.*, The era-interim reanalysis: Configuration and performance of the data assimilation system, *Q.J.R. Meteorol. Soc* **137**, 553 (2011).
- [37] <https://climate.copernicus.eu/climate-reanalysis/>.
- [38] M. Newman, *Networks: An Introduction* (Oxford University Press, New York, 2010).
- [39] M. E. J. Newman and R. M. Ziff, Efficient Monte Carlo Algorithm and High-Precision Results for Percolation, *Phys. Rev. Lett.* **85**, 4104 (2000).
- [40] J. Nagler, A. Levina, and M. Timme, Impact of single links in competitive percolation, *Nat. Phys.* **7**, 265 (2011).
- [41] J. Fan *et al.*, Universal gap scaling in percolation, *Nat. Phys.* **16**, 455 (2020).
- [42] H. A. Dijkstra, *Nonlinear Physical Oceanography: A Dynamical Systems Approach to the Large Scale Ocean Circulation and El Niño* (Springer Science and Business Media, New York, 2005).
- [43] See Supplemental Material at <http://link.aps.org/supplemental/10.1103/PhysRevE.104.064139> for the percolation analysis details for different variables, climate models, pressure levels and sub-periods. Demos such as the temporal evolution of some critical nodes, the statistical distributions of the temperature values and the selection of cluster boundaries are also discussed.
- [44] M. L. Salby, *Fundamentals of Atmospheric Physics* (Elsevier, London, 1996).
- [45] T. M. Pavelsky, J. Boé, A. Hall, and E. J. Fetzer, Atmospheric inversion strength over polar oceans in winter regulated by sea ice, *Clim. Dyn.* **36**, 945 (2011).
- [46] B. Bollobás, *Random Graphs* (Cambridge University Press, Cambridge, 2001).
- [47] B. B. Mandelbrot, *The Fractal Geometry of Nature*, 2nd ed. (Times Books, San Francisco, 1982).
- [48] H. E. Stanley, Cluster shapes at the percolation threshold: and effective cluster dimensionality and its connection with critical-point exponents, *J. Phys. A: Math. Gen.* **10**, L211 (1977).
- [49] B. Mandelbrot, How long is the coast of Britain? Statistical self-s and fractional dimension, *Science* **156**, 636 (1967).
- [50] E. B. Kraus and J. A. Businger, *Atmosphere-Ocean Interaction* (Oxford University Press, New York, 1994).
- [51] D. Achlioptas, R. M. D'Souza, and J. Spencer, Explosive percolation in random networks, *Science* **323**, 1453 (2009).
- [52] F. Radicchi and S. Fortunato, Explosive Percolation in Scale-Free Networks, *Phys. Rev. Lett.* **103**, 168701 (2009).
- [53] Y. S. Cho, S. Hwang, H. J. Herrmann, and B. Kahng, Avoiding a spanning cluster in percolation models, *Science* **339**, 1185 (2013).
- [54] R. M. Ziff, Explosive Growth in Biased Dynamic Percolation on Two-Dimensional Regular Lattice Networks, *Phys. Rev. Lett.* **103**, 045701 (2009).
- [55] J. Fan, M. Liu, L. Li, and X. Chen, Continuous percolation phase transitions of random networks under a generalized Achlioptas process, *Phys. Rev. E* **85**, 061110 (2012).
- [56] R. M. D'Souza, J. Gómez-Gardeñes, J. Nagler, and A. Arenas, Explosive phenomena in complex networks, *Adv. Phys.* **68**, 123 (2019).
- [57] M. Ghil and V. Lucarini, The physics of climate variability and climate change, *Rev. Mod. Phys.* **92**, 035002 (2020).